New precompound decay model: Angular distributions

M. Blann[1] and M. B. Chadwick[2]
[1]*7210E Calabria Court, San Diego, California 92122*
[2]*University of California, Theoretical Division, Los Alamos National Laboratory, Los Alamos, New Mexico 87545*
(Received 7 May 1997)

A new Monte Carlo precompound decay model is used to calculate double-differential spectra using an approach based on conservation of linear momentum between an incident nucleon and the three quasiparticles activated in the collisions of the equilibration process. The angular distribution theory is presented as it is applied to the individual three-exciton cascades of the precompound model. The importance of multiple precompound decay beyond two nucleons per nucleus is illustrated for ^{90}Zr(p,xn) reactions for incident protons up to 256 MeV. These components are shown to be important for extending the useful range of the precompound approach to energies beyond 80 MeV. The contribution to nucleon spectra due to hole conversion processes is illustrated. We compare results of the formulation described with experimental angular distributions for ^{90}Zr(p,xn) reactions at incident energies of 45, 80, and 160 MeV, and for the ^{90}Zr(p,xp) reactions at incident energies of 80, 160, and 200 MeV. Additionally, ^{208}Pb(p,xn) spectra at 7.5°, 30°, 60°, 120°, and 150° are compared with two experimental data sets for 256 MeV incident proton energy, and ^{90}Zr(p,xn) spectra at the same five angles are compared with predicted results for 256 MeV incident protons. At 256 MeV incident proton energy, the higher energy emission spectra are seriously overpredicted at 60°. All other results are reproduced quite well, including back-angle yields. The quasielastic peak measured at 7.5° at 256 MeV incident proton energy is shown to be in quite reasonable agreement with experimental results. [S0556-2813(98)03701-7]

PACS number(s): 24.10.Lx, 25.40.Hs

I. INTRODUCTION

A new precompound model [called hybrid Monte Carlo simulation (HMS)] using a Monte Carlo sampling method was recently introduced [1]. This approach follows nucleon-nucleon scattering such that only two and three quasiparticle scattering distributions (partial state densities) are involved. The latter have been shown to be consistent with the kinematic result of nucleon-nucleon scattering in nuclear matter [2,3]. This offers pedagogical improvements over earlier precompound formulations as discussed in [1]. The new formulation has no limit on the number of precompound nucleons emitted per reaction, and has been applied successfully at energies up to 400 MeV [4] for the calculation of excitation functions.

In the present work, we extend the HMS model to the calculation of double-differential cross sections. We do this by application of the method introduced in Ref. [5] based on the conservation of linear momentum of nucleons scattering to share the momentum between the resultant three quasiparticles. In this paper, which focuses on methods for determining the angular direction of scattered particles and holes, it is assumed that the scattered particle's energy is determined using the quasiparticle scattering distributions presented in Ref. [1]. In addition to intrinsic interest in the angular distributions of preequilibrium multistep scattering processes, incorporation of angular distributions into the HMS model is important for testing the model's ability to predict emission spectra, since much of the double-differential experimental data at higher energies are available for only a limited number of angles, prohibiting a reliable determination of experimental angle-integrated spectra.

In Sec. II we review the angular distribution formalism, and its application to the successive nucleonic cascades of the HMS model. Section III discusses some of the differences between the present model and intranuclear cascade (INC) formulations. In Sec. IV we present comparisons of the resulting model predictions with experimental double-differential spectra, and summarize our conclusions in Sec. V.

II. ANGULAR DISTRIBUTIONS

A. General

The angular distributions of emitted particles in our HMS calculations are obtained by following the directions of excited particles and holes in addition to their energy. To do this, the angular distributions from nucleon-nucleon scatterings within the nucleus must be determined. We make use of the angular distribution theory of Refs. [5,6]. This theory obtains the angular distribution in a scattering process by determining the accessible phase space, using state densities with linear momentum, with the effects of Pauli blocking and Fermi motion included.

By considering the linear momentum distribution of particles and holes, and applying momentum conservation, the authors of Ref. [5] derived the angular probability of a particle within a particle hole (p-h) exciton state being scattered to an angle θ,

$$G_n(K,k,\theta)=\frac{1}{4\pi}\,\frac{2a_n}{e^{a_n}-e^{-a_n}}\exp(a_n\cos\theta), \qquad (2.1)$$

with

$$a_n = \frac{3Kk}{2nm\epsilon_{\rm av}\zeta}, \tag{2.2}$$

where K is the total momentum of the p-h state, k is the momentum of the scattered nucleon which may be emitted, n is the number of excitons left after the scattering $(=p+h-1)$, m is the nucleon mass, and $\epsilon_{\rm av}$ is the average excitation energy of the remaining excitons, all energies and momenta being measured relative to the bottom of the nuclear well. The parameter $\zeta = \max(1, 9.3/\sqrt{E_{\rm em}})$, where $E_{\rm em}$ is the emission energy in the channel-energy frame, approximates quantum refraction and diffraction effects due to change of potential at the nuclear surface [5]. We assume that the effects asymptotically disappear above an 80 MeV channel energy, but at lower energies it increases the probability of back-angle scattering.

The derivation of the Eqs. (2.1) and (2.2) makes use of the central limit theorem to obtain a statistical Gaussian solution for the momentum distribution. The physical features of Eqs. (2.1) and (2.2) are discussed in the Appendix, including parallels with the Goldberger [7] (Kikuchi-Kawai [8]) equations for nucleon-nucleon scattering in nuclear matter, comparisons with nucleon momentum distributions obtained from other analyses, and a derivation showing that in the small-angle limit the average angular deviation following N scatterings is $\sqrt{N}$ times the average angular deviation in one scattering, as Feshbach has discussed using statistical arguments [9].

The above equations can be adapted for use in the present work as follows. First, the above formulas are only used for describing the directions of post-scattering particles after one particle interacts with a nucleon to produce two particles and one hole (hole scattering processes where a $1p2h$ state is produced are also included, though in the discussion below we concentrate on particle scattering processes for clarity). This is consistent with the HMS formalism, where excited particles are all tracked separately, each creating particle-hole excitations following a nucleon-nucleon collision. The kinematics of one particle creating subsequent particle-hole states $(1p \rightarrow 2p1h)$ is treated as occurring independently of any other particle-hole excitations that may exist within the nucleus. Second, in any scattering process the above equations can be used to determine the post-scattering directions of the two particles whether one or both of the particles are emitted immediately, or whether they undergo additional scatterings. Finally, the formulas are applied within a Monte Carlo approach. As is shown below, this has the significant advantage that the angular distributions and correlations of particles emitted through multiple preequilibrium emission processes (i.e., multiparticle fast preequilibrium ejectiles) can be straightforwardly determined.

Such multiple preequilibrium processes could not easily be treated within the deterministic (closed-form) formalism of Ref. [13], which was cause for an expected reduced reliability at incident energies above 80 MeV, with noticeable failings above around 160 MeV. These problems are likely to be present in any other precompound formulation which is limited to two precompound emissions per nucleus. The reasons for this may be seen by reference to Fig. 1, where we show single-differential neutron precompound spectra emitted following zero to $N-1$ other precompound nucleons for

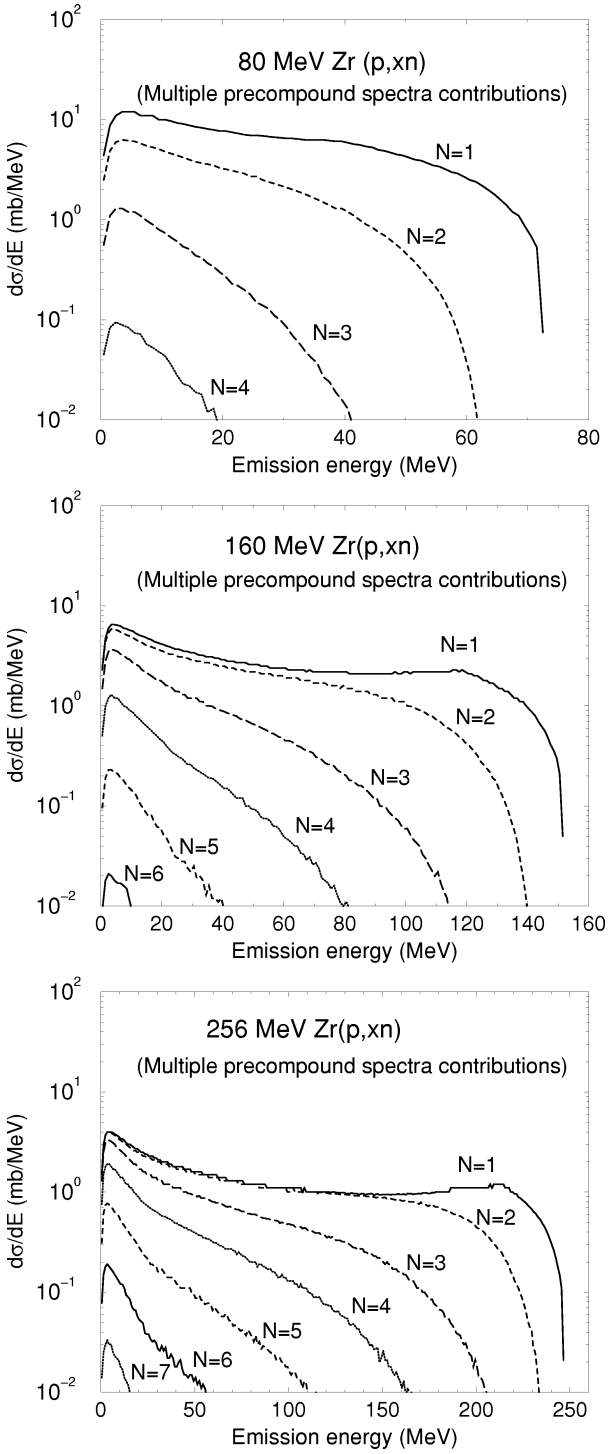

FIG. 1. Multiple precompound neutron emission contributions for 80, 160, and 256 MeV protons on ^{90}Zr. The solid curves ($N=1$) are the HMS-ALICE code spectra of the first precompound neutron emitted. The dashed curves ($N=2$) are the spectra of the neutrons emitted following the emission of either a preceding neutron or proton. The dashed curves ($N=3$) are the calculated neutron precompound spectra for a neutron emitted following two other precompound nucleons, the dotted curves ($N=4$) the spectra of a precompound neutron emitted following the emission of three other precompound nucleons, etc.

80, 160, and 256 MeV protons on ^{90}Zr targets, as predicted by the HMS-ALICE code. The increasing importance of precompound nucleons after the second (i.e., those emitted after two other nucleons) is clear. At 80 MeV, emission beyond two precompound nucleons is below the 10% level (which could be important for activation yields, but not too worrisome for single differential spectra). At 160 MeV, precompound spectra beyond multiplicity two are at the 30% or higher level at the lower range of the precompound spectra, where there are deficiencies in calculated precompound decay yields compared to measurements. As the incident proton energy increases, the relative contributions from multiplicity greater than 2 continues to increase, as is shown in the 256 MeV results.

We would emphasize that the ''$N=$'' numbers in Fig. 1 do not represent exciton numbers in terms of older exciton models; all emissions in the HMS model are treated with respect to $2p1h$ or $1p1h$ configurations. The ''$N=$'' numbers represent only the fact that there have been $N-1$ precompound nucleons emitted prior to the one for which the spectrum is being shown. The $N=1$ and $N=2$ results have a very high probability of representing the two nucleons from the initial scattering event, but either or both could also result from nucleons which have rescattered one or more times—and this will influence the angular distributions calculated. As the incident energy increases, we expect the $N=1$ and $N=2$ results to approach each other, except that the $N=2$ result must have its maximum energy reduced from that of $N=1$ by the binding energy of the first nucleon. This represents the fact that these emissions come primarily from the first scattering event, for which the energy partition is symmetric between the two particles after scattering, with the binding energy difference showing on the nucleon designated as the second to be emitted.

A simplification that follows from always considering $1p\rightarrow 2p1h$ events is that the average residual exciton excitation energy $\epsilon_{\rm av}$ in Eq. (2.2) can be determined using a Fermi-gas model. In Refs. [5,6] an analytic result was presented for the p-h average exciton energy based on equidistant single-particle energy levels, since the equivalent result for a Fermi gas (with a single-particle density increasing with the square root of the excitation energy) becomes intractable for large numbers of excitons. However, in the current approach one only needs the average excitation energy of very simple configurations, that is, $1p1h$ (for the particle emission from a $2p1h$ state), $1h$ (for particle emission from a $1p1h$ state), and $2h$ (for particle emission from a $1p2h$ state, produced by hole rescattering). In a Fermi gas model, we obtain

$$\epsilon_{\rm av}^{1p1h}=\begin{cases}\dfrac{\frac{2}{5}[V^{5/2}-(V-E)^{5/2}]+\frac{1}{3}E[V^{3/2}-(V-E)^{3/2}]}{\frac{2}{3}[V^{3/2}-(V-E)^{3/2}]} & \text{if } E<V,\\ \dfrac{3}{5}V+\dfrac{1}{2}E & \text{if } E\geqslant V,\end{cases} \tag{2.3}$$

$$\epsilon_{\rm av}^{1h}=\begin{cases}V-E & \text{if } E<V,\\ 0 & \text{if } E\geqslant V,\end{cases} \tag{2.4}$$

$$\epsilon_{\rm av}^{2h}=\begin{cases}V-(E/2) & \text{if } E\leqslant 2V,\\ 0 & \text{if } E>2V,\end{cases} \tag{2.5}$$

where E is the energy of the p-h configuration relative to the Fermi level, and V is the Fermi energy.

An attractive feature of using the angular distribution Eq. (2.1) is that it can be integrated analytically, so that angles can be sampled in a Monte Carlo approach using a closed-form expression. The probability of a particle being scattered to an angle θ is proportional to $G_n(K,k,\theta)\sin(\theta)$. To sample from this distribution, it must be integrated from $\theta=0$ to θ'—the sampled value for θ corresponds to the value of θ' for which the integral equals a random number R chosen between zero and unity. This then gives a sampled theta as

$$\theta'=a\cos(\ln\{\exp(a_r)-R[\exp(a_r)-\exp(-a_r)]\}/a_r). \tag{2.6}$$

B. Kinematical relations

Using the above considerations, we give expressions that are needed to determine the directions of particles and holes within a preequilibrium reaction. First, we consider the simplest case of the first scattering where the initial particle moves along the $\theta=0$ z axis, and determine the secondary particle directions (in the initial projectile's coordinate frame). Then we present more general relations where the initial particle moves in an arbitrary direction before a collision, for describing subsequent scatterings. Our notation always uses unprimed spherical coordinates to designate the coordinate frame defined by the incident projectile's direction (i.e., the $\theta=0$ z axis lies along the projectile's direction), which we designate the ''projectile coordinate system.''

The initial particle with momentum K_i scatters and forms a $2p1h$ state, with momentum $k_{2p1h}=K_i$. From this state, we consider the angular distribution of one of the final particles $p1$, with momentum k_{p1}, leaving a $1p1h$ state with momentum k_{1p1h} [Fig. 2(a)]. Equation (2.6) is used to sample the angular distribution, Eq. (2.1), for $G_2(k_{2p1h},k_{p1},\theta_{p1})$, and since there are two excitons remaining after selecting the particle's direction (θ_{p1},ϕ_{p1}), $a_{n=2}=3K_ik_{p1}/4m\zeta\epsilon_{\rm av}$ in Eq. (2.6), with $\epsilon_{\rm av}$ taken from Eq. (2.3). This gives a value for θ_{p1}, and ϕ_{p1} is chosen randomly between 0 and 2π.

The direction θ'_{p2} of the second particle, $(p2)$ from the remaining $1p1h$ state [Fig. 2(b)], with momentum k_{p2}, can

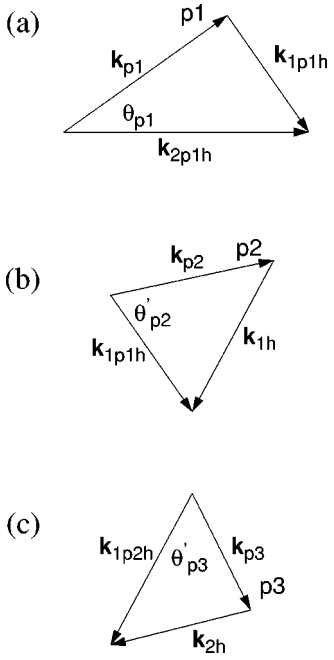

FIG. 2. Diagrams of momentum vectors for (a) scattering of a particle $p1$ from a $2p1h$ state; (b) scattering of a particle $p2$ from a $1p1h$ state; (c) scattering of a particle $p3$ from a $1p2h$ state.

then be obtained relative to the $1p1h$ momentum direction using Eq. (2.1) for $G_1(k_{1p1h},k_{p2},\theta'_{p2})$, sampling from Eq. (2.6) with $a_{n=1}=3k_{1p1h}k_{p2}/2m\zeta\epsilon_{\rm av}$, with $\epsilon_{\rm av}$ taken from Eq. (2.4). The angle ϕ'_{p2} is again chosen randomly between 0 and 2π. The $1p1h$ momentum is obtained from momentum conservation

$$k^2_{1p1h}=K_i^2+k^2_{p1}-2K_ik_{p1}\cos(\theta_{p1}), \tag{2.7}$$

and the direction of the $1p1h$ momentum relative to the projectile direction is

$$\theta_{1p1h}=\sin^{-1}\left[\frac{k_{p1}}{k_{1p1h}}\sin\theta_{p1}\right], \tag{2.8}$$

and $\phi_{1p1h}=\phi_{p1}+\pi$ for $\phi_{p1}\leqslant\pi$ and $\phi_{p1}-\pi$ for $\pi<\phi_{p1}\leqslant 2\pi$.

Since both θ'_{p2} and ϕ'_{p2} are determined relative to the $1p1h$ momentum direction, they need to be transformed into the projectile coordinate system to give the particle $p2$'s direction (θ_{p2},ϕ_{p2}). This can be done using Euler rotation matrices (see the Appendix): If the particle has a direction $(\theta'_{p2},\ \phi'_{p2})$ relative to the $1p1h$ direction, which in turn has a direction $(\theta_{1p1h},\phi_{1p1h})$ in the projectile coordinate system, then

$$\theta_{p2}=R_\theta(\theta_{1p1h},\phi_{1p1h},\theta'_{p2},\phi'_{p2}) \tag{2.9}$$

and

$$\phi_{p2}=R_\phi(\theta_{1p1h},\phi_{1p1h},\theta'_{p2},\phi'_{p2}), \tag{2.10}$$

where the rotation functions R_θ and R_ϕ are obtained from Eqs. (A9) and (A10) in the Appendix.

In this way, the directions of both particles in the frame of the projectile can be determined after a scattering event. However, the above equations assumed that the direction of the particle before scattering is in the $\theta=0$ direction, which is only the case for the first scattering event by the projectile; in subsequent scatterings the particle's direction before scattering is, in general, arbitrary, say, (θ_a,ϕ_a). In such cases, the above equations can be used, but after determining the final particle $p1$ and $p2$ directions relative to the (θ_a,ϕ_a) direction, they again must be rotated into the projectile coordinate frame using Eqs. (A9) and (A10), as was done in Eqs. (2.9) and (2.10), so that θ_{p1} is modified to $R_\theta(\theta_a,\phi_a,\theta_{p1},\phi_{p1})$, ϕ_{p1} is modified to $R_\phi(\theta_a,\phi_a,\theta_{p1},\phi_{p1})$, θ_{p2} is modified to $R_\theta(\theta_a,\phi_a,\theta_{p2},\phi_{p2})$, and ϕ_{p2} is modified to $R_\phi(\theta_a,\phi_a,\theta_{p2},\phi_{p2})$.

If both particles $p1$ and $p2$ were to be emitted, then the angular distributions (including correlations) of both particles (and of other nucleons emitted within this event) are automatically accounted for in such a multiple preequilibrium reaction.

The last type of scattering process to be considered is a hole scattering, forming a $1p2h$ state, from which the particle may be emitted. Physically, this corresponds to two bound nucleons below the Fermi level scattering with one another, one being scattered into the accessible hole level, and the other conserving energy and being scattered above the Fermi-level. Momentum conservation determines the $1h$ total momentum and direction before the scattering process, from Fig. 2(b). Equation (2.6) is used to sample the angular distribution, Eq. (2.1), for $G_2(k_{1p2h},k_{p3},\theta'_{p3})$, and since there are two holes remaining after selecting the particle's direction $(\theta'_{p3},\phi'_{p3})$, $a_{n=2}=3k_{1p2h}k_{p3}/4m\zeta\epsilon_{\rm av}$ in Eq. (2.6), with $\epsilon_{\rm av}$ taken from Eq. (2.5). The angle ϕ'_{p3} is chosen randomly between 0 and 2π. This determines the angle of the post-scattering particle relative to the initial hole' s direction, $(\theta'_{p3},\phi'_{p3})$, which subsequently must be rotated into the projectile coordinate system.

III. RELATIONSHIP TO OTHER MODELS

A. Intranuclear cascade models

1. General discussion

Here we briefly describe general aspects of the HMS model, with some reference to INC models, in order to answer the question as to how the model differs from the INC approach. In the following subsection these comparisons are made specifically as regards calculation of angular distributions, whereas here we concentrate on more general aspects.

The HMS model treats an incident nucleon entering a nucleus of known A,Z with known center-of-mass energy, to give an internal excitation E. There follows a two-body collision to give a two-particle, one-hole configuration sharing the excitation E with equal *a priori* probability between the three resulting ''excitons''; it was shown earlier [2] that the kinematics of nucleon-nucleon scattering in nuclear matter makes this a good approximation. Details of the selection of neutrons or protons as collision partners, and sampling techniques to select the energies of excitons, are described in Ref. [1] and we do not repeat these here.

From the three exciton distribution, using two- and three-exciton density expressions, we select the energy e of one particle above the Fermi energy; by the energy difference we

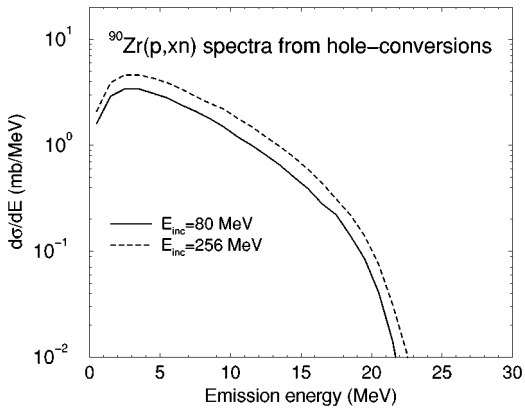

FIG. 3. Neutron spectra resulting from hole conversions for 80 and 256 MeV incident protons on ^{90}Zr.

know that the remaining particle-hole pair has $E-e$ units of energy, which may be shared between the particle and hole with equal *a priori* probability. (In the INC model, by preselecting the energy and angle of a struck nucleon below the Fermi energy, there is not the same averaging process in determining the momentum and energy of the two particles plus one hole.) The INC models follow the reaction processes in a three-dimensional geometry, while precompound models follow reactions in the energy space of the excitons.

If the nucleon selected above with energy e is unbound versus the binding energy BE(ν,A,Z) of the nucleon ν in the composite nucleus A,Z, then the usual precompound model rate expressions for emission into the continuum, and for rescattering (based on Pauli-corrected nucleon-nucleon scattering rates in nuclear matter) are used to determine whether nucleon ν is rescattered to make an additional $2p1h$ configuration at excitation e, or is emitted into the continuum with channel energy of $e-\mathrm{BE}(\nu,A,Z)$. If the latter, the energy of the particle from the residual $1p1h$ at energy $E-e$ is selected from the two-exciton function (i.e., equal probability) and the test for emission of this particle is applied, except that if the first nucleon emitted was a neutron, the binding energy used is BE(ν_2,$A-1$,Z), and if a proton, BE (ν_2,$A-1$,$Z-1$) is used. Each time there is a nucleon emission, the A and Z of the residues are appropriately decremented, so that correct binding energies are used for each nucleon, consistent channel energies result, and energy is conserved at each step of and over the entire cascade. The nucleons in the above description which rescatter start new $2p1h$ cascades, and the same process is repeated until all nucleons are bound; hole scatterings are then considered as an additional source of nucleon emission.

Hole conversion processes cannot contribute to the emission spectra at energies in excess of around 25 MeV, and should not contribute greatly to the intensity of even the lower energy spectra. Nonetheless, the contributions are not negligible, and will significantly impact activation yields. We show two spectra from hole conversion processes in Fig. 3. The magnitudes of these spectra should be compared with the spectra of all nucleons in Fig. 1 for a quantitative statement as to the contribution of hole conversions to the precompound spectra. Intranuclear cascade models do not treat hole conversion processes, and so this is one of the several differences between the HMS and INC models.

There are some differences with INC models which we note here which may be noticeable at the lower energies at which precompound models are used, and which are probably of more pedagogic than practical importance at the higher energies at which the INC models are generally applied. One such difference is that many INC codes either read in or, more often, have an internally set (i.e., ''hard-wired'') value for the average nucleon binding energy—which is then taken to be the binding energy of every nucleon emitted during the cascade. This may distort Coulomb barrier effects if, for example, there were multiple proton emissions, and means that energy is not conserved unless a post-cascade renormalization is performed using the sum over emitted nucleon channel energies, recoil energy, and correct experimental masses. Another difference, which may be significant at lower energies, is that many INC codes use a sharp cutoff value for the charged particle barrier: All charged particles reaching the surface above this energy are emitted; all below are rescattered. The present HMS model (as with all other precompound models) uses inverse reaction cross sections (usually from the nuclear optical model) to get the emission rate, thus giving a smoother spectrum with more realistic barrier dependence.

We point out the above differences as of pedagogical interest, and note that many INC codes give excellent results to relatively low energy. Most INC codes do use precompound models at some point of the cascade. There is sometimes a difficulty in determining the exciton number to use at this point. The present HMS model might be a good model to introduce into the INC codes, as it is also Monte Carlo, and would take each post-cascade nucleon, at some energy above the Fermi energy (and angle with respect to the beam direction) and treat its subsequent deexcitation in a consistent fashion, thus avoiding ambiguity as to exciton number. It would then follow each residual cascade particle and hole until all nucleons were particle bound, at which point transition would be made to the evaporation model. In the following subsection we discuss aspects of the HMS model with emphasis on the angular distributions, which are the main concern of this work, and comment on similarities and differences with respect to the INC model.

2. Angular distribution physics

The particle-hole formalism used in the HMS preequilibrium model differs from the methods used in intranuclear cascade models, though some of these differences are due to notation differences rather than differences in the underlying physical assumptions. The INC model randomly selects a bound nucleon for a scattering with a moving ''cascade'' particle above the Fermi level. The total momentum is then known before the scattering, and momenta of the two post-scattering cascading nucleons are randomly chosen (consistently with momentum and energy conservation requirements). The present model, instead, describes the scattering as a particle creating a $2p1h$ state with a total momentum equal to that of the particle before the scattering. This is, though, exactly analogous to the INC picture since the hole produced after the scattering event refers to the moving nucleon struck by the particle. An important feature of the HMS particle-hole formalism is that, rather than randomly choosing a bound nucleon for the scattering process, the ef-

fects of *all* bound nucleons that can act as collision partners are accounted for since an integration occurs over all the hole degrees of freedom [6].

The calculation of the post-scattering particle directions in a $1p \rightarrow 2p1h$ transition, described in Sec. II, can be interpreted as follows. After the momentum of the first particle $p1$ is selected according to the above angular distribution functions, the $1p1h$ state's momentum is known. From this, the direction of the second particle $p2$ is chosen relative to this $1p1h$ direction according to the angular distribution function. Now, in the INC model, once $p1$'s momentum is determined, then the $p2$ momentum is defined unambiguously from momentum conservation. But this is not the case here since we do not choose a specific nucleon for the scattering process, but rather we integrate over all possibilities. This is manifest in the fact that the varying possible hole momenta (corresponding to various struck nucleons) gives a spread in the momenta values of $p2$. Our formulas do preserve all the correlations in the final particle's momenta that would be expected from kinematics. The artificial case of the bound nucleons being stationary, without any Fermi momentum spread, is interesting to consider, since this can be simulated in the above equations by setting the Fermi energy to zero. In this case, after $p1$ is determined, the second particle is aligned completely with the $1p1h$ direction (its direction being defined uniquely at 90° to $p1$) since the forward-peaking a parameter for decay of the $1p1h$ state tends to infinity as the average excitation energy of the remaining one hole is zero.

B. Quantum multistep theories

Since the nuclear reactions studied in this paper have also been the focus of theoretical analyses based on quantum formalisms (particularly that of Feshbach, Kerman, and Koonin (FKK) [10]; see Refs. [11,12]), it is useful to make some comparisons between those works and the present approach.

Clearly the quantum approaches are based on a very different derivation to the present semiclassical work. In the FKK approaches, reaction probabilities are calculated after transition amplitudes are first determined. While statistical postulates are made that result in the canceling of certain interference terms in the multistep contributions of FKK theory, the final results preserve the forward-peaked angular distribution results obtained from distorted wave Born approximation (DWBA) theory, including interference and finite-size effects. The angular distributions calculated using the semiclassical methods in this paper agree with the experimental data to a degree comparable with the FKK predictions (see the next section); however, for lower incident energies than those studied in this paper (e.g., at 14 MeV) we expect the FKK predictions to be superior to those predicted by the present theory, since semiclassical assumptions do not hold at low energies.

An advantage of the present theory compared to the quantum theories is the ease with which a variety of nuclear reaction mechanisms can be calculated. For instance, the present theory allows an unlimited number of multiple preequilibrium emissions to be determined, whereas only a maximum of two preequilibrium ejectiles have been computed within quantum approaches [5] (particle emission beyond the second particle has not yet been determined due to the complexity of the formalism). The consequence of this is that the present theory can be applied to higher energies than can the FKK theory (in its current implementation), and that for incident energies in the region 160–250 MeV, the present theory predicts more accurate preequilibrium nucleon emission for outgoing energies in the range 20–50 MeV, where multiple preequilibrium emission is particularly important. This example is representative of the general differences in predictive capabilities between semiclassical and quantum preequilibrium formulations: The semiclassical models have their strength in their broad description of different reaction processes due to their ease of implementation; the quantum theories enable certain features to be determined that a semiclassical model can never predict (e.g., continuum analyzing powers, interference effects in angular distributions), but their computational implementation is often formidable.

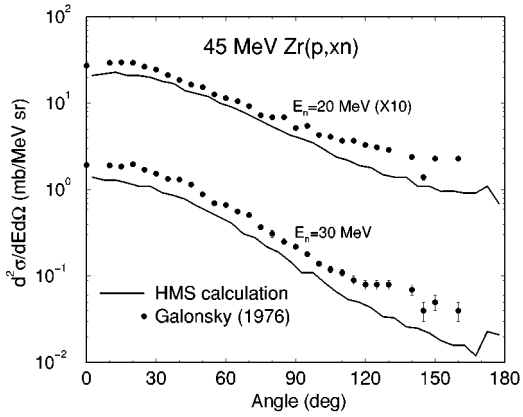

FIG. 4. Calculated and experimental angular distributions for the interaction of 45 MeV protons with ^{90}Zr. The solid circles are the experimental results of the MSU group of Galonsky *et al.* reported in Ref. [14]. The curves are the results of the HMS-ALICE code incorporating the theory of angular distributions described in Ref. [13]. Exit channel energies of 20 and 30 MeV are shown.

One interesting aspect of the present theory, which also applies to the FKK theory but not to some other quantum multistep formalisms [11], is the use of $1p1h$ state densities within expressions for the multistep transition processes. In the present theory, each subsequent multistep process is viewed as the creation of a new $2p1h$ state from which emission may occur, leaving a $1p1h$ state, with each new interaction assumed to occur independently of other particle-hole excitations. This assumption is consistent with the FKK approach, where multistep reactions are described as a convolution of one-step reactions, and differs from the exciton and hybrid semiclassical models.

IV. RESULTS AND DISCUSSION

Comparisons between calculated and experimental emission spectra are presented in this section. The variation of the calculated results from smooth curves in the figures represents statistical fluctuations from the Monte Carlo method used. For all results shown, 10×10^6 events were used in the calculations.

In Figs. 4–6 we compare results of the angular distribution theory under discussion with experimental results for

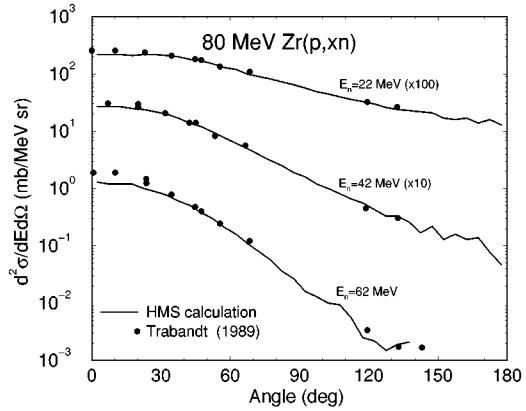

FIG. 5. Neutron angular distributions for 80 MeV protons on ^{90}Zr. Experimental results (solid circles) are from Ref. [15]. Calculated results are given by solid lines. Exit channel energies of 22, 42, and 62 MeV are shown.

(p,xn) reactions on ^{90}Zr targets at incident energies between 45 and 160 MeV. The energy distributions at five angles are compared for 256 MeV incident energy in Fig. 7.

In Fig. 8 we show similar energy distributions, but for a ^{208}Pb target for which two different groups have published experimental results, and we have replotted some of these data as angular distributions in Fig. 9. Angular distributions for protons emitted following 80, 160, and 200 MeV proton bombardment of ^{90}Zr are shown in Figs. 10–12.

The agreement of the shape of the calculated angular distributions or spectra at fixed angles with experimental yields tests the angular distribution theory under discussion in this work. The agreement in absolute yields tests the HMS model described in Ref. [1], where it was shown that inclusion of multiple precompound decay beyond two nucleons in the HMS model improved calculated spectra for high incident energies. In the results of this work we will see a tendency toward underprediction of yields for emitted nucleons below 40 MeV. This means that further improvements are needed in the HMS precompound model; it is an improvement over the earlier hybrid model, but there is room for further development. However, the test of the angular distribution theory under investigation lies in comparison of the calculated and

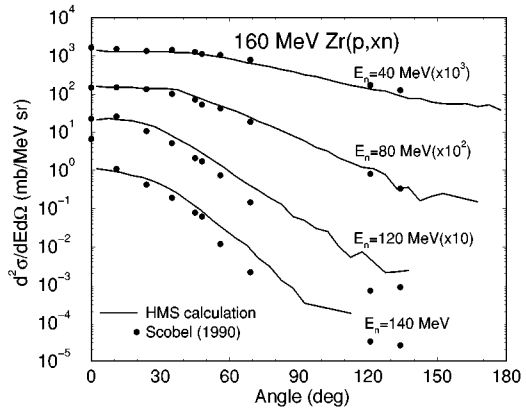

FIG. 6. Neutron angular distributions for 160 MeV protons incident on ^{90}Zr. Experimental results (solid circles) are from Ref. [16]. Calculated results are given by the solid lines for exit channel energies of 40, 80, 120, and 140 MeV.

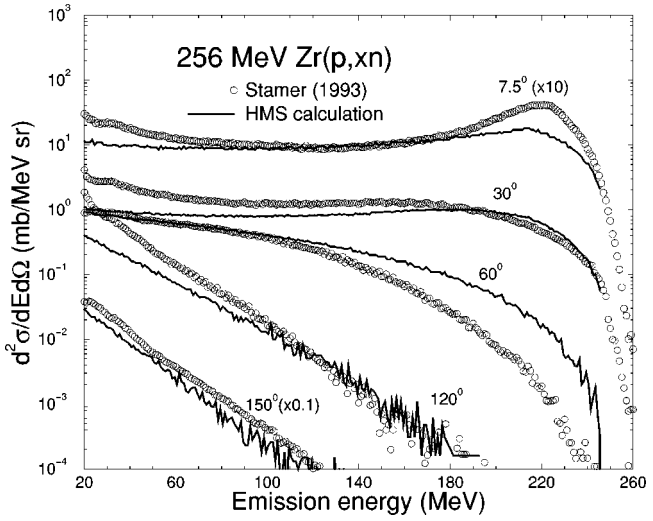

FIG. 7. Neutron energy spectra at fixed emission angles for 256 MeV protons incident on ^{90}Zr. Experimental results given by the open points are from Ref. [17]. Calculated results are for angles (lab) of 7.5°, 30°, 60°, 120°, and 150°. Both calculated and experimental results have been shifted by a factor of 10 (0.1) for the 7.5° (150°) spectra.

experimental shapes of angular distributions; errors in absolute normalization represent problems in the HMS model, not the angular distribution theory.

In showing experimental results for (p,xn) reactions at 80 and 160 MeV measured at the Indiana University Cyclotron Facility, we have omitted the points measured at angles between 80° and 114°. This is due to the detector having been collimated to an unknown degree (approximately by half) when a viewing port through a 115 cm concrete shielding block was incorrectly cut. As the points are all clearly in error in a systematic way, we chose to delete rather than to

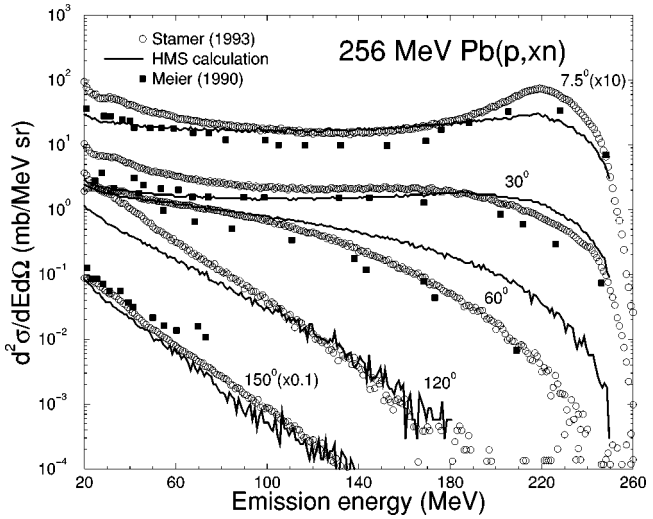

FIG. 8. Neutron energy spectra at fixed emission angles for 256 MeV protons on ^{208}Pb targets. Experimental results are given by open circles for results of Stamer *et al.* [17] and by solid squares for the results of Meier *et al.* [18]. Both sets of experimental spectra were measured at the LAMPF accelerator at LANL. Calculated results are shown as lines at lab angles of 7.5°, 30°, 60°, 120°, and 150°. Meier *et al.* did not report measurements at 120°.

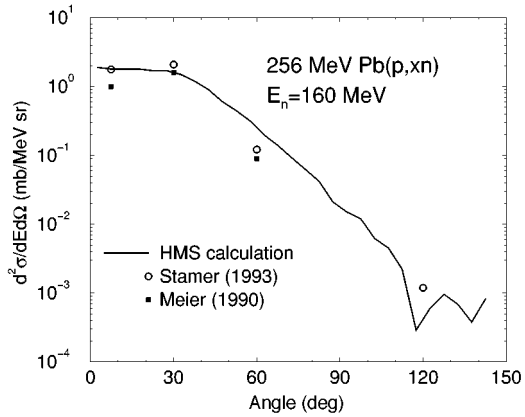

FIG. 9. Neutron angular distribution based on the data from Fig. 8. Points and lines are as in Fig. 8 for the data at 160 MeV emission energy. The experimental data due to Meier *et al.* [18] were interpolated from a smooth curve drawn through the experimental results.

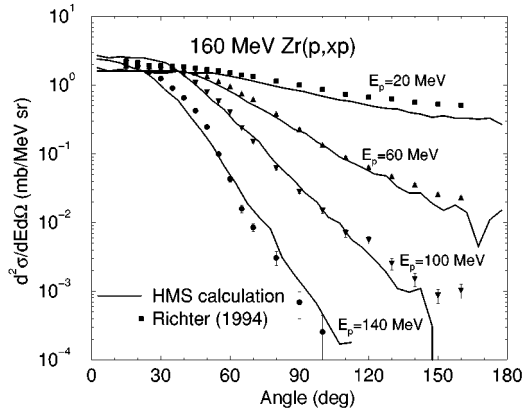

FIG. 11. Proton angular distributions for 160 MeV protons on ^{90}Zr. Experimental yields at 20, 60, 100, and 140 MeV (solid symbols) are from Richter *et al.* [19]. Calculated angular distributions are given by solid lines.

renormalize these experimental data points. Further discussion of this aspect of the experiment may be found in the original publications [15,16]. All other experimental points from the experiments cited are shown for the cases chosen.

The experimental angular distributions vary between those spanning one order of magnitude for emission energies far less than the incident proton energy, to those spanning five orders of magnitude for emission energies near to the incident proton energy. Rather without exception the shapes of the calculated angular distributions are in excellent agreement with the experimental data, confirming the value of the theory proposed in Ref. [5]. This is also true of yields at angles significantly beyond 90°, which have historically been grossly underestimated in semiclassical treatments.

The case which is less gratifying is that of the spectral yields for 256 MeV incident protons. We note that detector thresholds were set at 20 MeV for Ref. [17], and so perhaps yields at some of the lower energies may be uncertain. The results of Meier *et al.* [18], in Fig. 8, are different at the lower energies from the data of Ref. [17], and were measured using very low detector biases. The spectra, calculated at 60° for both the ^{90}Zr and ^{208}Pb targets for 256 MeV incident protons, are significantly harder than the experimental results. We do not see a similar failure in the 200 or 160 MeV (p,xp) results seen in Figs. 11 and 12, nor in the 160 MeV (p,xn) results of Fig. 6. We do not have an explanation for this, and it will be an interesting question as to why there should be a rapid decrease of accuracy of the angular distribution theory above 200 MeV incident energy. The angular distribution replot of the data of Fig. 8 shows that the discrepancy is not too important from a practical point of view, in that it does not affect a large part of the cross section. We are particularly pleased at the result for the quasielastic peak seen in the 7.5° spectrum of Figs. 7 and 8; this detail has historically been grossly overpredicted, and as a quite sharp peak, in earlier semiclassical models based on nucleon-nucleon scattering in a Fermi gas. The use of Gaussian momentum distributions implicit in the scattering kernel of Eqs. (2.1) and (2.2) results in a ''smearing out'' of the quasielastic peak compared to the results obtained using a sharp Fermi-gas momentum distribution. We are also very much encouraged by the excellent agreement with the experimental data at 120° and 150°, for as stated previously, back angle yields have heretofore been very difficult to predict with any acceptable degree of accuracy in semiclassical models and theories.

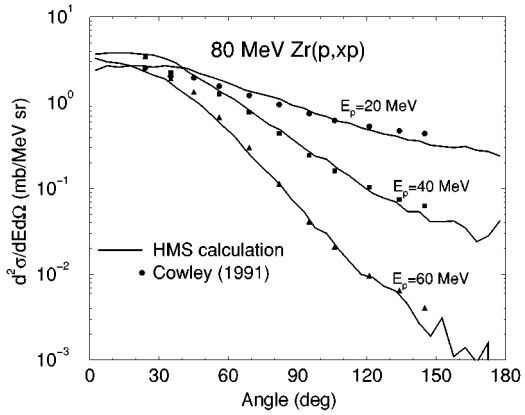

FIG. 10. Proton angular distributions for 80 MeV protons on ^{90}Zr. Experimental yields at 20, 40, and 60 MeV (open symbols) are from Cowley *et al.* [20]. Calculated results are given by solid lines.

V. CONCLUSIONS

We have coupled the angular distribution theory of Refs. [5,6] based on conservation of linear momentum between an incident nucleon and a three-quasiparticle final state, coupled to an equiprobability assumption, with the HMS precompound decay model based on successive two-body nucleon-nucleon scattering processes in nuclear matter, which always produce three-quasiparticle final states. For emitted nucleon energies above 80 MeV, the predicted angular distribution shapes are purely the result of the theory based on conservation of linear momentum between quasiparticle states, using a statistical Gaussian momentum distribution. For emitted energies below 80 MeV, a small semiempirical correction factor which had been determined in earlier work was incorporated without change. This factor, which asymptotically

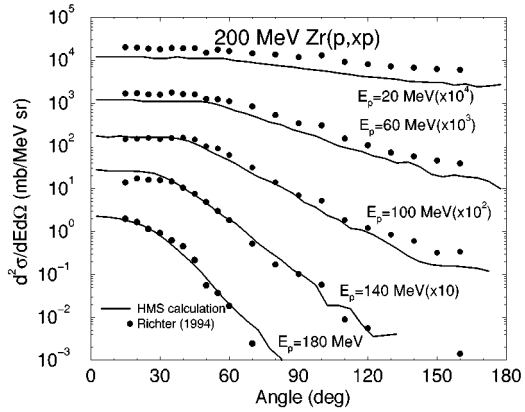

FIG. 12. Proton angular distributions for 200 MeV protons on ^{90}Zr. Experimental yields (closed circles) are from Richter *et al.* [19]. Calculated results are given by the solid curves. Results are shown for exit energies of 20, 60, 100, 140, and 180 MeV.

goes to unity at 80 MeV, is consistent with refractive effects which might be expected for lower energy nucleons encountering the nuclear surface due to change in potential, a semiclassical analogue of Snell's law [21].

The theory of Refs. [5,6] provides a very satisfactory predictive tool for the angular distributions of the fairly large number of experimental data sets shown, with some reservation for the 256 MeV data [17,18]. Extension of the HMS model to include angular distributions makes this combined approach a good candidate for incorporation for treatment of the precompound phase following INC calculations.

ACKNOWLEDGMENTS

One of the authors (M.B.) wishes to acknowledge support and hospitality during the course of this work from LLNL, LANL, ENEA (Bologna, Italy), Institute of Theoretical Physics, University of Frankfurt, and support of the Alexander von Humboldt Foundation.

APPENDIX

1. Angular distribution theory

a. Relation to Goldberger (Kikuchi and Kawai) nuclear matter results

Our work makes use of the theory of Ref. [5] to determine angular distributions in nucleon-nucleon scattering, making use of the variation of the accessible phase space with scattering angle to determine the distributions. It is, perhaps, useful to summarize the findings of Ref. [6] connecting these results to those obtained by Goldberger [7], and rewritten by Kikuchi and Kawai [8], for nucleon-nucleon scattering in nuclear matter. Reference [6] showed that when Fermi-gas states are used, and the $1p1h$ phase space determined using an ''exact'' convolution in energy and momentum space (with a momentum- and energy-conserving delta function), the Kikuchi-Kawai result is obtained. However, the present work, instead, uses the statistical solution for the $1p1h$ momentum-dependent phase space. For large numbers of excitons, the statistical solution was shown to tend to the ''exact'' solution. Our present work uses the statistical (Gaussian) solution for a number of reasons: (1) It is compact and based on a very general derivation, (2) the results were shown in Ref. [5] to provide a physical basis for the experimentally based Kalbach angular distribution systematics [22], and (3) even in the nonstatistical limit, there are arguments (see the next subsection) indicating that a Gaussian momentum distribution is a reasonable approximation.

b. Momentum distribution discussion

The angular distribution theory of Ref. [5] used the central limit theorem to determine the momentum distribution of a p-h state, obtaining a Gaussian result:

$$M(p,h,E,\mathbf{K}) = \frac{1}{(2\pi)^{3/2}\sigma^3}\exp(-K^2/2\sigma^2), \qquad \text{(A1)}$$

where the momentum cutoff σ, representing the width of the distribution, is obtained by determining the average-squared value of the exciton momentum projections on the direction of $\mathbf{K}$, giving $\sigma^2=(p+h)2m\epsilon_{\rm av}/3$. Fermi motion and Pauli blocking are accounted for in the determination of $\epsilon_{\rm av}$ since particles are above the Fermi level, holes below it. In the present paper, equations are presented for $\epsilon_{\rm av}$ within a Fermi-gas model, and analogous results based on an equidistant single-particle model were presented in Ref. [5]. However, it is instructive to consider the nonstatistical limit of this result for the momentum distribution of one nucleon below the Fermi level. This is equivalent to the result for one hole, and so $h=1$ and $p=0$ in the above equation. Additionally, the average kinetic energy in a Fermi-gas model is $3\epsilon_F/5$, giving a nucleon momentum distribution proportional to $\exp[-K^2/(4m\epsilon_F/5)]$. But this is exactly the same as the leading term in the momentum distribution obtained experimentally. For instance, Araseki and Fujita [23] parametrize the nuclear momentum distribution as $[\exp(-p^2/p_0^2)+\epsilon_0\exp(-p^2/q_0^2)]$, where p is the momentum, $p_0=\sqrt{2/5}k_F$, $\epsilon_0=0.03$, and $q_0=\sqrt{3}p_0$. The dominant $[\exp(-p^2/p_0^2)]$ term is identical to our result.

This, therefore, provides further support for the angular distribution theory we use, and provides some justification for its application even when the number of excitons is small.

c. Angular width in multistep scattering

Feshbach [9] has discussed the increasing angular spread in nuclear scattering with increasing scattering steps within a multistep direct preequilibrium context: If the angular distribution for the single-step cross section peaks in the forward direction with angular width $\delta\theta_1$, the multistep process for N steps is predicted to lead again to a forward peak, with width $\sqrt{N}\delta\theta_1$. It is interesting that the formalism of Ref. [5], as summarized in Eqs. (2.1) and (2.2), gives this same result.

To show this, the average value of θ_N in N-step scattering must be determined. The integrals that must be solved to find this value cannot be done analytically, but the result can be approximated if the average value of $\cos\theta_N$ is first determined:

$$\langle\cos\theta_N\rangle=\frac{\int_0^\pi \cos\theta_N\, e^{a_n\cos\theta_N} 2\pi\sin\theta_N d\theta_N}{\int_0^\pi e^{a_n\cos\theta_N} 2\pi\sin\theta_N d\theta_N}, \qquad \text{(A2)}$$

which, for large a_n (small-angle scattering), gives $\langle\cos\theta_N\rangle = 1-1/a_n$. Thus $\langle\sin\theta_N\rangle=\sqrt{2/a_n}$, and therefore for small-angle N-step scattering we obtain an average angular width of $\delta\theta_N=\sqrt{2/a_n}$. But since $a_n\propto 1/n$ [Eq. (2.2)], and $N=n/2$, we obtain, in the small-angle scattering limit,

$$\delta\theta_N=\sqrt{N}\,\delta\theta_1, \qquad \text{(A3)}$$

in agreement with Feshbach's prediction.

2. Rotation matrices

In the implementation of our HMS model, it is frequently necessary to transform a particle's direction relative to one coordinate frame into another (usually the ''projectile coordinate system'' defined by the projectile's motion). To do this we use Euler rotation matrices.

Suppose a particle has a direction (θ_2,ϕ_2) with respect to an axis that in turn has a direction (θ_1,ϕ_1) relative to the projectile coordinate system. The Euler rotation usually written as ''α,'' representing a rotation about the z axis through an angle α, can be associated with ϕ_1, and the Euler rotation ''β,'' representing a subsequent rotation of the z axis about the new y axis, can be associated with θ_1.

Since we wish to determine the particle's direction within the ''original'' projectile coordinate system (whose angles are the unprimed variables θ and ϕ), a rotation $\mathsf{R}_z(-\phi)\mathsf{R}_y(-\theta)$ must be applied to the direction (θ_2,ϕ_2), where

$$\mathsf{R}_z(\phi)=\begin{pmatrix}\cos\phi_1 & \sin\phi_1 & 0\\ -\sin\phi_1 & \cos\phi_1 & 0\\ 0 & 0 & 1\end{pmatrix} \qquad \text{(A4)}$$

and

$$\mathsf{R}_y(\theta)=\begin{pmatrix}\cos\theta_1 & 0 & -\sin\theta_1\\ 0 & 1 & 0\\ \sin\theta_1 & 0 & \cos\theta_1\end{pmatrix}. \qquad \text{(A5)}$$

Thus, the direction in the projectile coordinate system is

$$\begin{pmatrix}\sin\theta\cos\phi\\ \sin\theta\sin\phi\\ \cos\theta\end{pmatrix}=\begin{pmatrix}\cos\phi_1 & -\sin\phi_1 & 0\\ \sin\phi_1 & \cos\phi_1 & 0\\ 0 & 0 & 1\end{pmatrix}\begin{pmatrix}\cos\theta_1 & 0 & \sin\theta_1\\ 0 & 1 & 0\\ -\sin\theta_1 & 0 & \cos\theta_1\end{pmatrix}\begin{pmatrix}\sin\theta_2\cos\phi_2\\ \sin\theta_2\sin\phi_2\\ \cos\theta_2\end{pmatrix} \qquad \text{(A6)}$$

$$=\begin{pmatrix}\cos\phi_1\cos\theta_1\sin\theta_2\cos\phi_2-\sin\phi_1\sin\theta_2\sin\phi_2+\sin\theta_1\cos\phi_1\cos\theta_2\\ \sin\phi_1\cos\theta_1\sin\theta_2\cos\phi_2+\cos\phi_1\sin\theta_2\sin\phi_2+\sin\theta_1\sin\phi_1\cos\theta_2\\ -\cos\phi_2\sin\theta_2\sin\theta_1+\cos\theta_1\cos\theta_2\end{pmatrix}. \qquad \text{(A7)}$$

Thus, the angles θ and ϕ can be obtained as

$$\theta=R_\theta(\theta_1,\phi_1,\theta_2,\phi_2), \quad \text{and} \quad \phi=R_\phi(\theta_1,\phi_1,\theta_2,\phi_2), \qquad \text{(A8)}$$

where

$$R_\theta(\theta_1,\phi_1,\theta_2,\phi_2)=\cos^{-1}[-\cos\phi_2\sin\theta_2\sin\theta_1+\cos\theta_1\cos\theta_2] \qquad \text{(A9)}$$

and

$$R_\phi(\theta_1,\phi_1,\theta_2,\phi_2)=\tan^{-1}\left[\frac{\sin\phi_1\cos\theta_1\sin\theta_2\cos\phi_2+\cos\phi_1\sin\theta_2\sin\phi_2+\sin\theta_1\sin\phi_1\cos\theta_2}{\cos\phi_1\cos\theta_1\sin\theta_2\cos\phi_2-\sin\phi_1\sin\theta_2\sin\phi_2+\sin\theta_1\cos\phi_1\cos\theta_2}\right]. \qquad \text{(A10)}$$

[1] M. Blann, Phys. Rev. C **54**, 1341 (1996).
[2] M. Blann and H. K. Vonach, Phys. Rev. C **28**, 1475 (1983).
[3] J. Bisplinghoff Phys. Rev. C **33**, 1569 (1986).
[4] M. V. Mebel, A. S. Iljinov, C. Grandi, G. Reffo, and M. Blann, Nucl. Instrum. Methods Phys. Res. A **398**, 324 (1997).
[5] M. B. Chadwick and P. Oblozinsky, Phys. Rev. C **50**, 2490 (1994).
[6] M. C. Chadwick and P. Oblozinsky, Phys. Rev. C **46**, 2028 (1992).
[7] M. L. Goldberger, Phys. Rev. **74**, 1269 (1948).
[8] K. Kikuchi and M. Kawai, *Nuclear Matter and Nuclear Reactions* (North Holland, Amsterdam, 1968) p. 44.
[9] H. Feshbach, *Theoretical Nuclear Physics* (Wiley, New York, 1992), p. 40.

[10] H. Feshbach, A. Kerman, and S. Koonin, Ann. Phys. (N.Y.) **125**, 429 (1980).
[11] R. Bonetti, A. J. Koning, J. M. Akkermans, and P. E. Hodgson, Phys. Rep. **247**, 1 (1994).
[12] A. J. Koning and J. M. Akkermans, Phys. Rev. C **47**, 724 (1993).
[13] M. B. Chadwick, P. G. Young, D. C. George, and Y. Watanabe, Phys. Rev. C **50**, 996 (1994); M. B. Chadwick, S. Chiba, K. Niita, T. Muruyama, and A. Iwamoto, *ibid.* **52**, 2800 (1995).
[14] M. Blann, R. R. Doering, A. Galonsky, D. M. Patterson, and F. E. Serr, Nucl. Phys. **A257**, 15 (1976).
[15] M. Trabandt, W. Scobel, M. Blann, B. A. Pohl, R. C. Byrd, C. C. Foster, R. Bonetti, and S. M. Grimes, Phys. Rev. C **39**, 452 (1989).
[16] W. Scobel, M. Trabandt, M. Blann, B. A. Pohl, B. R. Remington, R. C. Byrd, C. C. Foster, R. Bonetti, C. Chiesa, and S. M. Grimes, Phys. Rev. C **41**, 2010 (1990).
[17] S. Stamer, W. Scobel, W. B. Amian, R. C. Byrd, R. C. Haight, J. L. Ullmann, R. W. Bauer, M. Blann, B. A. Pohl, J. Bisplinghoff, and R. Bonetti, Phys. Rev. C **47**, 1647 (1993).
[18] M. M. Meier, C. A. Goulding, G. L. Morgan, and J. Ullmann, Nucl. Sci. Eng. **104**, 339 (1990); **110**, 289 (1992).
[19] W. A. Richter, A. A. Cowley, G. C. Hillhouse, J. A. Stander, J. W. Koen, S. W. Steyn, R. Lindsay, R. E. Julies, J. J. Lawrie, J. V. Pilcher, and P. E. Hodgson, Phys. Rev. C **49**, 1001 (1994).
[20] A. A. Cowley, A. van Kent, J. J. Lawrie, S. V. Fortsch, D. M. Whittal, J. V. Pilcher, F. D. Smit, W. A. Richter, R. Lindsay, I. J. van Heerden, R. Bonetti, and P. E. Hodgson, Phys. Rev. C **43**, 678 (1991).
[21] M. Blann, W. Scobel, and E. Plechaty, Phys. Rev. C **30**, 1493 (1984).
[22] C. Kalbach, Phys. Rev. C **37**, 2350 (1988).
[23] H. Araseki and T. Fujita, Nucl. Phys. **A439**, 681 (1985).